# Role of Ion Kinetic Physics in the Interaction of Magnetic Flux Ropes

A. Stanier,* W. Daughton, and L. Chacón
*Los Alamos National Laboratory, Los Alamos, New Mexico 87545, USA*

H. Karimabadi
*SciberQuest, Inc., Del Mar, California 92014, USA*

J. Ng, Y.-M. Huang, A. Hakim, and A. Bhattacharjee
*Center for Heliophysics, Princeton Plasma Physics Laboratory, Princeton, New Jersey 08543, USA*
(Received 21 July 2015; published 21 October 2015)

To explain many natural magnetized plasma phenomena, it is crucial to understand how rates of collisionless magnetic reconnection scale in large magnetohydrodynamic (MHD) scale systems. Simulations of isolated current sheets conclude such rates are independent of system size and can be reproduced by the Hall-MHD model, but neglect sheet formation and coupling to MHD scales. Here, it is shown for the problem of flux-rope merging, which includes this formation and coupling, that the Hall-MHD model fails to reproduce the kinetic results. The minimum sufficient model must retain ion kinetic effects, which set the ion diffusion region geometry and give time-averaged rates that reduce significantly with system size, leading to different global evolution in large systems.

DOI: 10.1103/PhysRevLett.115.175004 PACS numbers: 52.35.Vd, 94.30.cp

Magnetic reconnection relaxes stressed magnetic fields by changing field-line connectivity in highly conducting plasmas. The associated energy release is considered important for many magnetized plasma phenomena in nature [1,2], but the theoretical question of how reconnection proceeds fast enough to explain this energy release in large systems is not fully understood.

Most of the previous simulation studies have addressed this question by initializing the simulations with isolated kinetic-scale current sheets, finding that the reconnection rate in collisionless plasmas is independent of both the system size [3–6] and the mechanism that breaks the frozen-in condition, including specific details of the electron [7–9] and ion kinetic physics [10,11] that are not present in two-fluid models. However, in nature, such current sheets take a finite time to form, and involve the interplay between magnetohydrodynamic (MHD) and kinetic scale physics. The magnetic island coalescence problem [12–16] is a simple reconnection test problem that includes many key features present in real systems: the buildup of magnetic energy, the dynamic formation of the current sheet, and the onset and the cessation of reconnection. Such islands are two-dimensional representations of magnetic flux ropes, a fundamental building block of magnetized plasmas [17–19].

Reconnection during island coalescence is characteristically bursty, since it is coupled with the global motions of the islands, and thus it is suitable to consider the time averaged reconnection rate. A recent fully kinetic study [16] found that the average rate scales as $\langle E_R \rangle \propto (\lambda/d_i)^{-1/2}$, where $d_i$ is the ion-skin depth and $\lambda$ is the equilibrium current thickness, a proxy for the system size. However, no explanation for the strong system-size scaling has been given, and due to the computational difficulty of modeling large islands it has remained unclear how these predictions will compare with the commonly used two-fluid models, such as the Hall-MHD model. Several studies [20,21] have considered strongly driven Hall-MHD reconnection and reported significant system-size dependence, but impose an *ad hoc* driving.

In this Letter, it is demonstrated that the Hall-MHD model fails to reproduce any of the key features from the equivalent fully kinetic simulations of island coalescence: the peak and average reconnection rates, the dependence on the initial ion to electron temperature ratio $T_{i0}/T_{e0}$, the pileup strength of the magnetic field, and the global island motion. In the Hall-MHD model, reconnection proceeds until the islands fully coalesce, and the peak and average rates have a weak dependence on system size. In contrast, a hybrid model that retains kinetic ion physics with massless fluid electrons reproduces the broad ion diffusion region, and the associated reduction of the pileup magnetic field and outflow velocity of the fully kinetic model. In hybrid and fully kinetic models, reconnection in large systems is significantly slower, so that the islands bounce [12,14] and have a different global evolution from the Hall-MHD model.

The essential physics responsible for this discrepancy relates to the anisotropic and agyrotropic nature of the ion pressure tensor, in which a large contribution is due to the ion meandering orbits [11,22,23] within the weak magnetic field regions of the reconnection layer. These orbits give rise to large gradients in the ion pressure tensor, which are not treated correctly in current fluid models. While the

 

existence of broader ion layers has been mentioned in the literature [9–11,24–27], their importance has been missed due to the extensive use of highly extended current sheets for the initial conditions. Here, it is shown that ion pressure tensor effects play a primary role in controlling the magnetic field pileup and outflow velocity, and thus determine the reconnection rate and the global evolution of this system. These results have conceivable implications for real reconnecting systems in which coupling of micro- to macroscale physics is important, such as Earth's magnetosphere.

All of the simulations described are initialized with a magnetic island equilibrium [28], with similar parameters to a recent study [16]. The initial magnetic potential is

$$A_z = B_0\lambda \ln\left[\cosh\left(x/\lambda\right) + \epsilon\cos\left(y/\lambda\right)\right], \tag{1}$$

where $\epsilon = 0.4$ and $B_0$ is the asymptotic field. For a thermal pressure balanced equilibrium, the density profile is

$$n = n_b + \frac{n_0(1-\epsilon^2)}{\left[\cosh\left(x/\lambda\right) + \epsilon\cos\left(y/\lambda\right)\right]^2}, \tag{2}$$

where $n_b = 0.2n_0$ is the background density, $n_0$ is the central Harris-sheet density enhancement in the limit $\epsilon = 0$, and the initial temperatures are constrained as $T_{i0} + T_{e0} = B_0^2/(2\mu_0 n_0 k_B)$. The ratio of ion to electron current carrying velocities is set equal to the temperature ratio $T_{i0}/T_{e0}$ to give an exact Vlasov equilibrium in the fully kinetic case, see, e.g., Ref. [29]. The simulation domain is $x \in [-\pi\lambda, \pi\lambda]$, $y \in [-2\pi\lambda, 2\pi\lambda]$. In this study, the system size $\lambda/d_i$ and the initial temperature ratio $T_{i0}/T_{e0}$ are varied. Additional code specific parameters are as follows, for the Hall-MHD model [30–32], the electron inertia is set to zero $d_e = 0$, the resistivity $\eta = 10^{-5}\mu_0 d_i v_{A0}$, the hyperresistivity $\eta_H = 10^{-4}\mu_0 d_i^3 v_{A0}$, and the ion viscosity $\mu = 10^{-2} m_i n_0 d_i v_{A0}$. For the hybrid model (see Ref. [33] and references therein), $d_e = 0$, $\eta = 10^{-5}\mu_0 d_i v_{A0}$, $\eta_H = 10^{-3}\mu_0 d_i^3 v_{A0}$, and the ratio of ion plasma frequency to gyrofrequency $\omega_{pi}/\Omega_{ci} = 2000$. For the fully kinetic particle-in-cell (PIC) model [34], the ratio of electron frequencies $\omega_{pe}/\Omega_{ce} = 2$, and the mass ratio $m_i/m_e = 25$ ($d_e = d_i/5$). The results discussed are not sensitive to these choices, e.g., of $\eta_H$ or $\omega_{p\{i/e\}}/\Omega_{c\{i/e\}}$. For all codes, an initial sinusoidal magnetic perturbation of amplitude $\delta B = 0.1B_0$ is used to start the merging [16]. A movie showing the evolution of the current density (color scale) and magnetic flux during the merging for the $\lambda = 10d_i$ simulation can be found in the Supplemental Material [35].

Figure 1 shows the reconnection rate $E_R$ against the global-Alfvén time $t/t_A = tv_{A0}/(4\pi\lambda)$, from the Hall-MHD, hybrid, and fully kinetic simulations with $\lambda = 5d_i$ and $T_{i0} = T_{e0}$. Here, $E_R$ is calculated as in Ref. [16]

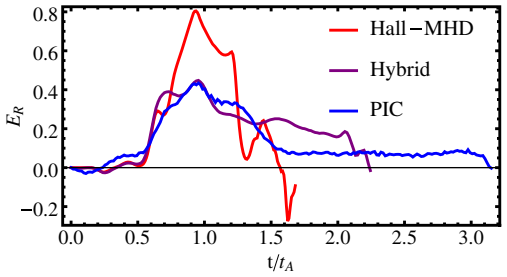


FIG. 1 (color online). Reconnection rate $E_R$ against $t/t_A$ for the Hall-MHD (red), hybrid (purple), and fully kinetic PIC (blue) runs with $\lambda = 5d_i$ and $T_{i0} = T_{e0}$.

$$E_R = \frac{1}{v_{Am}B_m}\partial_t[A_{zX} - A_{zO}], \tag{3}$$

where $A_{zX/O}$ is $A_z$ evaluated at the $X/O$ magnetic null point, $B_m$ is the maximum initial field between the islands, and $v_{Am} = B_m/\sqrt{n_0\mu_0 m_i}$.

The peak reconnection rate for the hybrid simulation ($E_R = 0.455$) is in good agreement with the fully kinetic PIC result (0.435), whereas the Hall-MHD run (0.805) overestimates the peak rate by $\approx 85\%$. Additional runs (not shown) confirm the peak rates do not depend on electron-scale physics, but the late time rate ($t/t_A \gtrsim 1.5$, which differs between the hybrid and PIC codes) does depend weakly on $m_i/m_e$ in the PIC runs, or $\eta_H$ for the hybrid runs.

Figure 2 shows the peak rates $E_R$ and the average rates $\langle E_R\rangle$ where $\langle\rangle$ is the average over $1.5\tau_A$ (chosen as a secondary island forms in the $\lambda = 5d_i$ Hall-MHD simulation after this time, see below) against system size $\lambda/d_i$. In the Hall-MHD model, $E_R$ flattens earlier ($\approx 10d_i$) than in the hybrid and PIC runs, so the overestimate of $E_R$ grows to more than a factor of 3 for $\lambda = 25d_i$. The average rates in the hybrid runs, $\langle E_R\rangle \propto (\lambda/d_i)^{-0.65}$, and PIC runs,

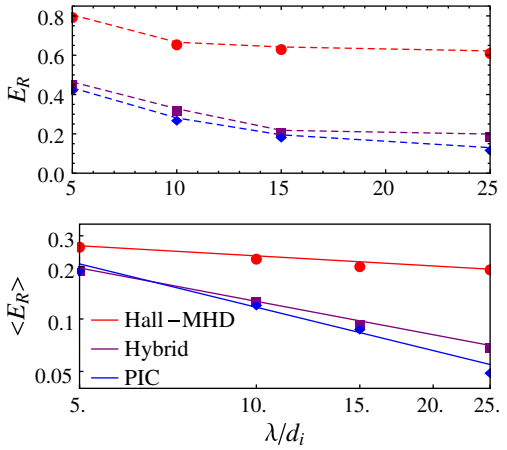


FIG. 2 (color online). Top: peak rates ($E_R$) against system size ($\lambda/d_i$) for the Hall-MHD (red), hybrid (purple), and PIC (blue) runs. Bottom: average rates ($\langle E_R\rangle$) over $1.5\tau_A$. The top (bottom) plot has linear (logarithmic) axes.

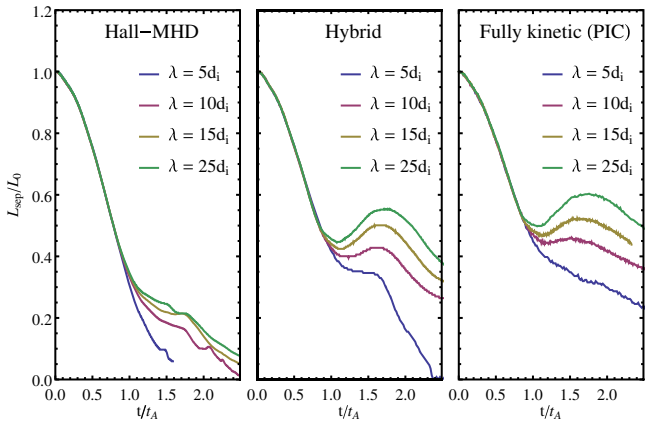


FIG. 3 (color online). Normalized $O$ point separation ($L_{\rm sep}/L_0$) against $t/t_A$ for the Hall-MHD (left), hybrid (middle), and PIC (right) runs. Shown for each code are system sizes $\lambda = 5d_i$ (blue), $\lambda = 10d_i$ (pink), $\lambda = 15d_i$ (gold), and $\lambda = 25d_i$ (green).

$(\lambda/d_i)^{-0.8}$, reduce significantly more steeply with $\lambda/d_i$ than in the Hall-MHD model, $(\lambda/d_i)^{-0.25}$. This precise scaling with $\lambda/d_i$ for the PIC runs differs from that reported in Ref. [16], and we find in general that these scalings depend on the aspect ratio of the simulation domain, which influences the dynamical interaction of the islands. Here, this aspect ratio is kept constant between all three codes as the system size is varied.

The differences in the rates have important consequences for the global evolution of the system. Figure 3 shows the separation of the $O$ points, at the center of the magnetic islands, normalized by the initial separation $L_0$ as a function of $t/t_A$. There are clear differences between the Hall-MHD and kinetic ion codes after the initial ideal phase $t \gtrsim 0.8$. For the Hall-MHD model (left panel) there is no clear reversal in the $O$ point separation, and the islands in these simulations tend to fully coalesce as they first approach each other. It must be noted that the $\lambda = 5d_i$ run forms a secondary magnetic island at late time $t \approx 1.6$, which stagnates reconnection and does cause the islands to bounce. However, since this bouncing is due to a separate issue, this evolution is not considered to compare fairly with the other runs. For the hybrid and PIC runs, there is reversal in the O point motion for system sizes $\lambda \geq 10d_i$. The islands are unable to coalesce on the first approach due to the slower reconnection rates, and so bounce off each other. There is good agreement between the hybrid and PIC runs, except for the late time $t \gtrsim 2$ behavior that depends on the electron scale physics, see above.

Figure 4 shows how the kinetic ion physics affects the geometry of the ion diffusion region. The $z$ component of the ion momentum equation can be expressed as an ion Ohm's law in normalized form

$$E_z' = \frac{d_i}{n}[\partial_t(nv_{iz}) + \boldsymbol{\nabla}\cdot(n\mathbf{v}_i v_{iz})] + \frac{d_i}{n}\boldsymbol{\nabla}\cdot\boldsymbol{P}_{iz} + F_{\rm coll,z}, \qquad (4)$$

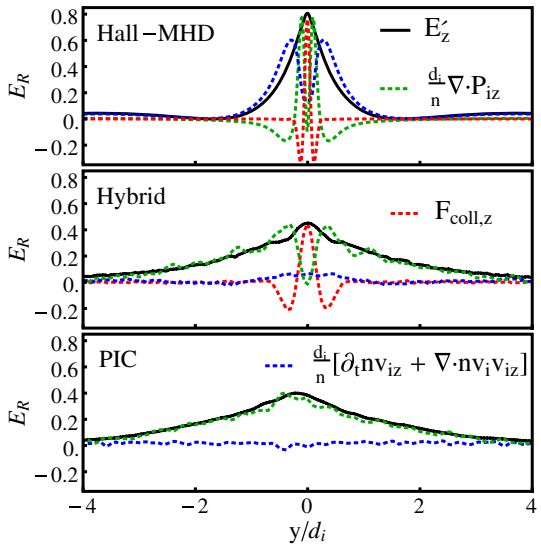


FIG. 4 (color online). $E_z'$ (black) across the ion diffusion region ($x = 0$) for the Hall-MHD (top), hybrid (middle), and PIC (bottom) runs at peak $E_R$. Contributions from ion inertia (blue), pressure tensor (green), and frictional terms (red). For all, $\lambda = 5d_i$, $T_{i0} = T_{e0}$.

where $E_z' = (\boldsymbol{E} + \boldsymbol{v}_i \times \boldsymbol{B})\cdot\hat{z}$ is the nonideal electric field, $\boldsymbol{P}_{iz} = \bar{\bar{\boldsymbol{P}}}_i \cdot \hat{z}$ is due to the ion-pressure tensor, and $F_{\rm coll,z} = \eta j_z - \eta_H \nabla^2 j_z$ is the resistive and hyperresistive friction. When the right-hand side of Eq. (4) is negligible the ideal-MHD Ohm's law is recovered, and the magnetic field is frozen in to the ion fluid. However, $E_z'$ becomes nonzero within the ion diffusion region, where the ion bulk flows decouple from the field. The contributions to $E_z'$ (black curves) in cuts across the ion diffusion region are shown in Fig. 4. For the Hall-MHD model (top) the thickness of the ion diffusion region, taken to be the full width at half maximum of $E_z'$, is $\delta_i = 0.62d_i$. $E_z'$ is primarily supported by bulk ion inertia (blue dotted line), whereas ion pressure tensor effects (green) and frictional effects (red, mainly hyperresistivity) are only significant very close to the X point and so do not set the ion diffusion region thickness. For this Hall-MHD model, $\boldsymbol{P}_{iz} = -\mu\boldsymbol{\nabla}v_{iz}$ is a simple collisional ion viscosity.

In contrast, the hybrid (middle) and PIC (bottom) runs have a broader ion diffusion region ($\delta_i \approx 2.4d_i$, $2.8d_i$ respectively), where $E_z'$ is primarily supported by gradients in the off-diagonal elements of the ion-pressure tensor (green). Here, $\boldsymbol{P}_{iz}$ is collisionless and directly calculated from the distribution of ion particle velocities.

Figure 5 (top) shows the agyrotropy $A\emptyset_i$, a scalar measure of the departure of $\boldsymbol{P}_i$ from cylindrical symmetry with respect to the magnetic field (see Appendix A of Ref. [36] for the full definition), from the hybrid run. In a cut across the inflow axis ($x = 0$), there is a significant agyrotropy, $A\emptyset_i = 0.2$, that peaks at $y = \pm 1.9d_i$ upstream of the X point. Also shown (white solid) is the trajectory of

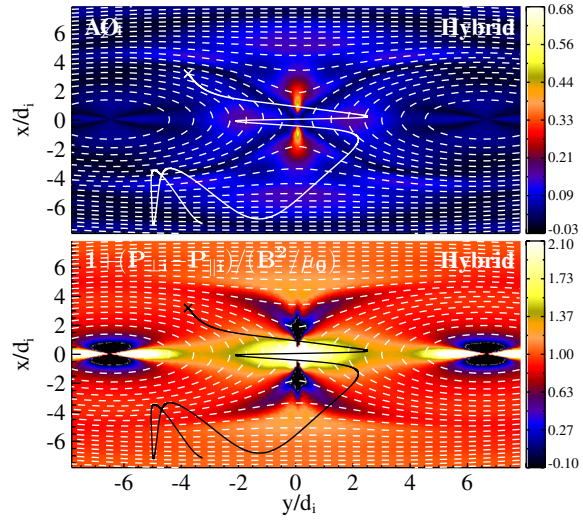


FIG. 5 (color online). Top: ion agyrotropy $A\emptyset_i$ (color scale), flux contours (white, dashed), and ion test-particle orbit (white solid) starting from "×" with thermal velocity. Bottom: firehose parameter $1 + (p_{i\perp} - p_{i\parallel})/(B^2/\mu_0)$ (color scale), flux (white), and trajectory (black). From hybrid run with $\lambda = 5d_i$, $T_{i0} = T_{e0}$.

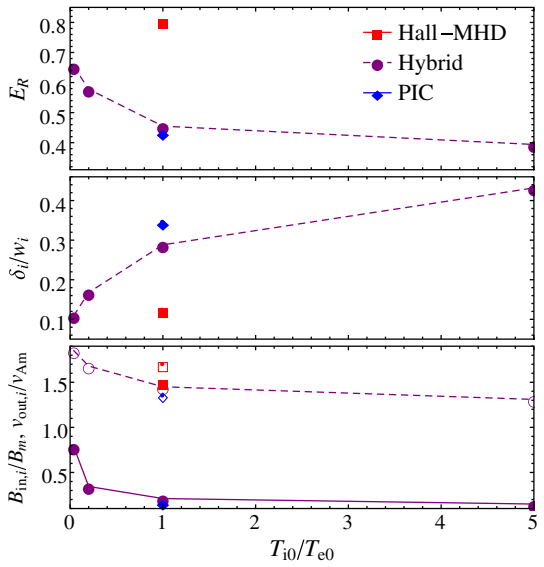


FIG. 6 (color online). Top: peak rate $E_R$. Middle: aspect ratio of the ion nonideal region, $\delta_i/w_i$. Bottom: inflow field $B_{\mathrm{in},i}/B_m$ (hollow, dashed) and outflow velocity $v_{\mathrm{out},i}/v_{Am}$ (filled, solid). Results are from $\lambda = 5d_i$ using the Hall-MHD model (red squares) and fully kinetic PIC runs (blue diamonds) with $T_{i0}/T_{e0} = 1$, and hybrid runs (purple circles) with $T_{i0}/T_{e0} = 0.04, 0.2, 1, 5$.

a typical ion test particle starting at $(x, y) = (3.2, -3.76)$ with local thermal velocity, and advanced using the electromagnetic fields of the hybrid run. The ion exhibits "meandering-type" [7,11,22] crossing orbits with reversal points at $y_r \approx \pm 2.2d_i$, before it enters the outflow region and is magnetized. This distance is in agreement with both the region of significant inflow agyrotropy and the extent of the pressure tensor term in the ion Ohm's law (middle panel of Fig. 4). Also of interest is the significant agyrotropy $A\emptyset_i \approx 0.6$ along $y = 0$, suggesting that nongyrotropic pressure effects contribute to the force balance in the exhaust, but it is not as visible for large $\lambda/d_i$ (not shown).

The reversal distance $y_r$ and extent of regions with significant $A\emptyset_i$ decrease with $T_{i0}$, and decrease in proportion to the global system for larger $\lambda/d_i$ (not shown). However, ion kinetic effects remain manifest on global scales via pressure anisotropy ($p_{i\parallel}/p_{i\perp} \neq 1$). First, a wedge shaped region with a firehose parameter $1 + (p_{i\perp} - p_{i\parallel})/(B^2/\mu_0) \gtrsim 1.3$ that is outside of $y_r$ between the $X$ and O points in Fig. 5 is caused by perpendicular heating and coincides with the region of flux pileup. Second, along $y = 0$ the exhaust approaches the firehose instability threshold $1 + (p_{i\perp} - p_{i\parallel})/(B^2/\mu_0) \approx 0$, reducing tension in the reconnected field, and thus may reduce the outflows with respect to the inflow Alfvén speed (see below and Ref. [37]). The $A\emptyset_i$ and firehose parameter in the PIC runs (not shown) agree well with those in the hybrid runs.

Figure 6 shows the peak rate $E_R$, aspect ratio $\delta_i/w_i$, inflow field $B_{\mathrm{in},i}/B_m$ and outflow velocity $v_{\mathrm{out},i}/v_{Am}$ from the Hall-MHD, hybrid, and kinetic runs with $\lambda = 5d_i$. Since $y_r$ decreases with $T_{i0}$, the role of kinetic ions is studied by varying $T_{i0}/T_{e0}$ in the hybrid simulations. The Hall-MHD and PIC results are plotted for $T_{i0}/T_{e0} = 1$, although there is no noticeable temperature dependence in these quantities for the Hall-MHD model. For $T_{i0}/T_{e0} = 1$, the Hall-MHD model fails to reproduce $E_R$, $\delta_i/w_i$, $B_{\mathrm{in},i}/B_m$, or $v_{\mathrm{out},i}/v_{Am}$ of the PIC runs, while the hybrid run captures all of these features reasonably well. As $T_{i0}/T_{e0}$, and thus $y_r$, is reduced in the hybrid runs, it might be expected that the Hall-MHD results are in better agreement. Indeed, $\delta_i/w_i$ and $B_{\mathrm{in},i}/B_m$ are closer to the Hall-MHD results, and the contribution to $E_z'$ from ion inertia becomes non-negligible (not shown). However, the Hall-MHD model still overestimates both $E_R$ and $v_{\mathrm{out},i}/v_{Am}$ with respect to the cold-ion hybrid, presumably as the hybrid ion pressure tensor does not remain cold or isotropic due to ion heating within the reconnection layer and outflow.

The magnetic island coalescence problem includes key features of real reconnecting systems: magnetic field pileup, current sheet formation, and coupling between the MHD and kinetic scales. In this Letter, it is shown the widely used Hall-MHD fluid model is unable to reproduce such features from fully kinetic PIC simulations. For this problem, kinetic ions are required to describe the structure of the ion pressure tensor, broader ion diffusion regions, pileup magnitude, ion outflow velocity, and thus the reconnection rates and global behavior of the PIC runs. The thickness of the ion diffusion region agrees with the extent of ion meandering orbits, and is associated with significant ion pressure agyrotropy and anisotropy. This physics is missing in the Hall-MHD model and work is presently being done to approximate such effects in more

advanced fluid models [38,39]. The importance of kinetic ions has been argued previously [26], but for an isolated current sheet the peak rate was similar to that in the Hall-MHD model. We also note that although electron kinetics were not crucial for this problem, studies in Harris geometry have found them important to set the length of electron layers [37,40], and they can affect global behavior through formation of secondary magnetic islands. The most important consequence of the present study is the different global evolution of the system between the Hall-MHD and kinetic ion codes. In the Hall-MHD model the islands fully coalesce on first approach, whereas hybrid and PIC islands with $\lambda \geq 10d_i$ bounce off each other. The importance of such ion kinetic effects are conceivably generic to many real reconnecting systems where the coupling between macro- to microscale physics is important.

This work is supported by NSF Grant No. AGS-1338944, and used resources provided by the Los Alamos National Laboratory Institutional Computing Program, which is supported by the U.S. Department of Energy National Nuclear Security Administration under Contract No. DE-AC52-06NA25396.

*stanier@lanl.gov

[1] E. Priest and T. Forbes, *Magnetic Reconnection* (Cambridge University Press, Cambridge, England, 2000).
[2] E. G. Zweibel and M. Yamada, Annu. Rev. Astron. Astrophys. **47**, 291 (2009).
[3] M. A. Shay, J. F. Drake, B. N. Rogers, and R. E. Denton, Geophys. Res. Lett. **26**, 2163 (1999).
[4] J. D. Huba and L. I. Rudakov, Phys. Rev. Lett. **93**, 175003 (2004).
[5] W. Daughton and H. Karimabadi, Phys. Plasmas **14**, 072303 (2007).
[6] A. Stanier, A. N. Simakov, L. Chacón, and W. Daughton, Phys. Plasmas **22**, 010701 (2015).
[7] M. Hesse, K. Schindler, J. Birn, and M. Kuznetsova, Phys. Plasmas **6**, 1781 (1999).
[8] M. A. Shay and J. F. Drake, Geophys. Res. Lett. **25**, 3759 (1998).
[9] J. Birn, J. F. Drake, M. A. Shay, B. N. Rogers, R. E. Denton, M. Hesse, M. Kuznetsova, Z. W. Ma, A. Bhattacharjee, A. Otto, and P. L. Pritchett, J. Geophys. Res. **106**, 3715 (2001).
[10] M. A. Shay, J. F. Drake, B. N. Rogers, and R. E. Denton, J. Geophys. Res. **106**, 3759 (2001).
[11] R. Horiuchi and T. Sato, Phys. Plasmas **1**, 3587 (1994).
[12] D. Biskamp and H. Welter, Phys. Rev. Lett. **44**, 1069 (1980).
[13] J. C. Dorelli and J. Birn, Geophys. Res. Lett. **108**, 1133 (2003).
[14] D. A. Knoll and L. Chacón, Phys. Plasmas **13**, 032307 (2006).
[15] D. A. Knoll and L. Chacón, Phys. Rev. Lett. **96**, 135001 (2006).
[16] H. Karimabadi, J. Dorelli, V. Roytershteyn, W. Daughton, and L. Chacón, Phys. Rev. Lett. **107**, 025002 (2011).
[17] E. N. Parker, Astrophys. J. **174**, 499 (1972).
[18] X. Sun, T. P. Intrator, L. Dorf, J. Sears, I. Furno, and G. Lapenta, Phys. Rev. Lett. **105**, 255001 (2010).
[19] W. Daughton, V. Roytershteyn, H. Karimabadi, L. Yin, B. J. Albright, B. Bergen, and K. J. Bowers, Nat. Phys. **7**, 539 (2011).
[20] X. Wang, A. Bhattacharjee, and Z. W. Ma, Phys. Rev. Lett. **87**, 265003 (2001).
[21] R. Fitzpatrick, Phys. Plasmas **11**, 937 (2004).
[22] T. W. Speiser, J. Geophys. Res. **70**, 4219 (1965).
[23] M. M. Kuznetsova, M. Hesse, and D. Winske, Geophys. Res. Lett. **105**, 7601 (2000).
[24] L. Yin and D. Winske, Phys. Plasmas **10**, 1595 (2003).
[25] H. Karimabadi, J. D. Huba, D. Krauss-Varban, and N. Omidi, Geophys. Res. Lett. **31**, L07806 (2004).
[26] H. Karimabadi, D. Krauss-Varban, J. D. Huba, and H. X. Vu, Geophys. Res. Lett. **109**, A09205 (2004).
[27] N. Aunai, G. Belmont, and R. Smets, Geophys. Res. Lett. **116**, A09232 (2011).
[28] V. M. Fadeev, I. F. Kvabtskhava, and N. N. Komarov, Nucl. Fusion **5**, 202 (1965).
[29] K. Schindler, *Physics of Space Plasma Activity* (Cambridge University Press, Cambridge, England, 2006).
[30] L. Chacón, J. Phys. Conf. Ser. **125**, 012041 (2008).
[31] L. Chacón, Phys. Plasmas **15**, 056103 (2008).
[32] Y.-M. Huang, A. Bhattacharjee, and B. P. Sullivan, Phys. Plasmas **18**, 072109 (2011).
[33] H. Karimabadi, B. Loring, P. O'Leary, A. Majumdar, M. Tatineni, and B. Geveci, in *Proceedings of the Conference on Extreme Science and Engineering Discovery Environment: Gateway to Discovery, XSEDE '13* (ACM, New York, 2013), pp. 57:1–57:8.
[34] K. J. Bowers, B. J. Albright, L. Yin, W. Daughton, V. Roytershteyn, B. Bergen, and T. J. T. Kwan, J. Phys. Conf. Ser. **180**, 012055 (2009).
[35] See Supplemental Material at http://link.aps.org/supplemental/10.1103/PhysRevLett.115.175004 for a movie showing the coalescence process for the $\lambda = 10d_i$ case.
[36] J. Scudder and W. Daughton, Geophys. Res. Lett. **113**, A06222 (2008).
[37] A. Le, J. Egedal, J. Ng, H. Karimabadi, J. Scudder, V. Roytershteyn, W. Daughton, and Y.-H. Liu, Phys. Plasmas **21**, 012103 (2014).
[38] L. Wang, A. H. Hakim, A. Bhattacharjee, and K. Germaschewski, Phys. Plasmas **22**, 012108 (2015).
[39] J. Ng, Y. M. Huang, A. Hakim, A. Bhattacharjee, A. Stanier, W. Daughton, L. Wang, and K. Germaschewski, Phys. Plasmas (to be published).
[40] W. Daughton, J. Scudder, and H. Karimabadi, Phys. Plasmas **13**, 072101 (2006).